PERGAMON

International Journal of Multiphase Flow 27 (2001) 885–910

International Journal of Multiphase Flow

www.elsevier.com/locate/ijmulflow

The prediction of dispersed flows boundaries in liquid–liquid and gas–liquid systems

Neima Brauner *

School of Engineering, Tel-Aviv University, Tel-Aviv 69978, Israel

Received 18 October 1999; received in revised form 21 September 2000

Abstract

A unified approach for predicting the transition to dispersed flow patterns in gas–liquid and liquid–liquid systems is suggested. It is based on the revised models for predicting the maximal drop size in a turbulent field which account for the holdup of the dispersed phase. Examining the range of applicability of the various models for transition to dispersed flow indicates that it is determined by the Eötvös number, $Eo_D = \Delta\rho g D^2/8\sigma$. Comparisons with available experimental data for gas–liquid and oil–water systems show that these models are capable of predicting the effects of fluids' physical properties, tube diameter and inclination. The models suggest a non-monotomic effect of the tube diameter on the critical fluids' flow rates, which implies that the up-scaling of data should be approached with care. © 2001 Elsevier Science Ltd. All rights reserved.

1. Introduction

A dispersion of two immiscible fluids, where one of the fluids forms a continuous phase and the other is dispersed in it, is a flow pattern which is often observed in liquid–liquid and gas–liquid systems. In oil–water two-phase flows, there are water-in-oil (w/o) and oil-in-water (o/w) dispersions. Emulsion is a stable dispersion of fine droplets (w/o or o/w), which usually involves the presence of surfactants inhibiting coalescence of the dispersed droplets. In gas–liquid systems, the bubbly flow patterns are dispersions of gas in a continuous liquid phase, whereas the mist pattern is a dispersion of liquid droplets in the gas core.

Dispersions can be obtained at low flow rates as a result of mixing in a device used to introduce the two fluids into the tube. For sufficiently low holdup of the dispersed phase, low density

* Tel.: +972-3-6408127; fax: +972-3-6407334.
E-mail address: brauner@eng.tau.ac.il (N. Brauner).

0301-9322/01/$ - see front matter © 2001 Elsevier Science Ltd. All rights reserved.
PII: S0301-9322(00)00056-2

contrast between the continuous and dispersed phases, or weak gravitational field, coalescence is not prominent even in horizontal tubes and the dispersion may sustain far downstream. However, dispersions will always form in sufficiently intense motions of two immiscible fluids, where the dispersive forces are due to the turbulent energy dissipation. The prediction of dispersed flow boundaries is then based on the modeling of the turbulent dispersive forces balancing with the resistant forces due to surface tension and gravity field.

For horizontal and slightly inclined gas–liquid flows Taitel and Dukler (1976) have modeled the dispersed bubble boundary by equating the turbulent breakage forces with the buoyant forces tending to keep the gas at the top of the pipe. These forces were evaluated for a configuration of stratified gas–liquid flow and the shear velocity was used for representing the turbulent velocity fluctuations. Although the stratified flow and dispersed bubble flow patterns do not share a common boundary, the Taitel and Dukler (1976) model has been successfully applied for predicting the transition to dispersed bubble flow in horizontal and near-horizontal pipes.

For vertical and off-vertical inclined gas–liquid systems, Taitel et al. (1980) and Barnea et al. (1985) have suggested Hinze's (1955) model for the breakage of drops or bubbles in a uniform and homogeneous turbulent field. According to this model the turbulence level in the liquid phase should be sufficiently high to overcome the surface tension forces, which resist deformation and breakup and to disperse the gas phase into small and stable spherical bubbles. Calderbank's (1958) correction for the effect of the dispersed phase holdup on the maximal bubble diameter and Brodkey (1969) model for the maximal size of stable spherical drops were used to obtain a criterion for transition to dispersed bubble flow. This model was later extended (Barnea, 1987) by introducing the effect of buoyant forces in horizontal and shallow inclinations on the stable drop size, so that the Hinze's mechanism could be applied for the whole range of pipe inclinations. However, these models are suitable for predicting the transition to dispersed bubble flow only for relatively low gas superficial velocities. With increasing the gas flow rate, the models deviate from the experimental boundary, showing an incorrect trend of a decline in the transitional liquid flow rate. As a remedy, Taitel et al. (1980) and Barnea (1987) have suggested that at high gas holdup, the model based on Hinze's mechanism should be overruled by the criterion of a maximal packing density of dispersed gas bubbles. Transition then takes place at a maximal in situ holdup ($\varepsilon_d = 0.52$, see Fig. 1). Chen et al. (1997) recently proposed a model which considers the balance between the liquid turbulent kinetic energy and bubbles' surface energy as a criterion for transition to dispersed bubbles. This model predicts a monotonous increase in the liquid transitional flow rate with increasing the gas flow rates, but it underestimates the critical liquid rate at low gas rates.

Hinze's mechanism for breakage of droplets in turbulent flow was suggested also for predicting transition to fully dispersed patterns in liquid–liquid flows (Brauner and Moalem Maron, 1992a,b). It was shown (Brauner, 1998) that by adjustment of the free parameter in Calderbank's (1958) correction for the effect of the holdup on the maximal drop size, it is possible to follow the experimental data of transition to o/w and w/o dispersions (emulsions) as observed in various oil–water systems. However, the criterion of maximum dispersed phase packing ($\varepsilon_d = 0.52$) is not useful for liquid–liquid systems. At high flow rates the flow patterns of o/w dispersion and w/o dispersion share a common boundary along the phase inversion curve. Experiments show that the dispersed phase holdup can exceed 74% (corresponding to close packing of equally sized spheres). A primary factor which seems to affect the critical holdup at phase inversion is the liquid viscosity

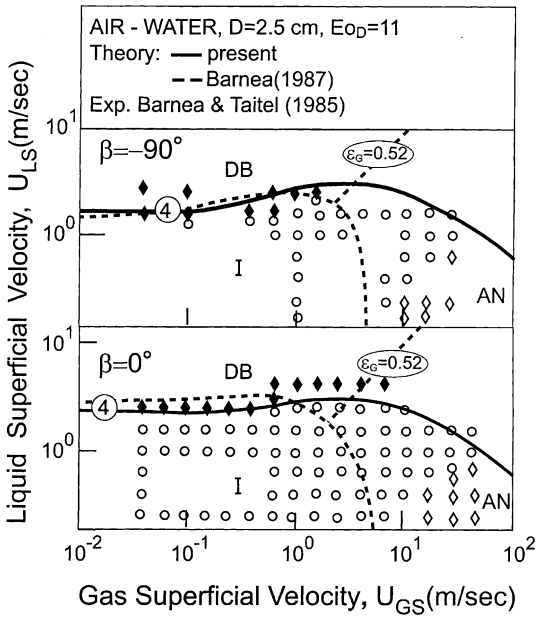

Fig. 1. Comparison of the H-model predictions with experimental data for air–water flow in vertical and horizontal tubes, $D = 2.5$ cm. ◆ – dispersed bubbles (DB); ○ – intermittent and slug (I); ◇ – annular (AN); ■ – stratified–wavy (SW).

ratio. The holdup of the dispersed oil droplets along the phase inversion curve increases with increasing the oil viscosity and reaches a value of $\approx$ 85–90% for viscous oils (Arirachakaran et al. (1989), Brocks and Richmond (1994)).

In this paper, the various mechanisms for dispersion formation are considered. Models suggested are revised and extended to yield a unified approach for predicting the transitions to dispersed flow patterns in a variety of gas–liquid and liquid–liquid systems. The study is aimed at elaborating the effect of fluids' physical properties, tube diameter and inclination on the fluids' flow rates required for stabilizing fully dispersed flow patterns. Examining the range of applicability of the various mechanisms and models for transition to dispersed flow indicates that it depends on the Eötvös number ($Eo_D = \Delta\rho g D^2/8\sigma$). This dimensionless parameter has been already shown to be important in determining the stratified flow characteristics and its stability boundaries (Brauner and Moalem Maron (1992a,b, 1998); Brauner et al. (1998)) and in modeling the drift velocity of drops and bubbles (e.g., Zukoski, 1966; Clift et al., 1978; Grace et al., 1978).

2. Criterion based on Hinze's (1955) model (H-model)

2.1. Hinze's model for dilute dispersions

Most of the models for predicting the size of bubbles or drops in a turbulent flow field are based on the Kolmogorov (1949)–Hinze (1955) model for emulsification in turbulent flow. Using

dimensional arguments they show that the splitting of a drop (or a bubble) in turbulent flow depend on the critical Weber number, $We_{crit} = \tau d_{max}/\sigma$, which represents the ratio between the external force (τ) that tends to deform the drop, and the counteracting surface tension force. For the sake of clarity of the herein proposed extended model, physical arguments and underlying assumptions of Hinze's model are briefly reviewed.

In turbulent flows, the spatial regions where viscous shear is effective are small compared to the size of the large drops and the dominant external stress is the dynamic pressure of turbulent eddies of size d. In this case, We_{crit} (and the associated maximal drop size, d_{max}) evolves from a balance between the turbulent kinetic energy and the drop surface energy (Hinze, 1955)

$$\frac{\rho_c u'^2}{2} \simeq \frac{4\sigma}{d_{max}}, \tag{1}$$

where ρ_c is the density of the continuous phase. In isotropic and homogeneous turbulence, the turbulent kinetic energy can be related to the rate of turbulent energy dissipation (per unit mass of the continuous phase), $\bar{e}$

$$u'^2 = 2(\bar{e}d_{max})^{2/3} \tag{2.1}$$

provided

$$l_k = \left(\frac{\eta_c^3}{\rho_c^3 \bar{e}}\right)^{1/4} \ll d_{max} \ < 0.1D, \tag{2.2}$$

where η_c is the continuous phase viscosity, l_k is the Kolmogorov microscale and $0.1D$ represents the length scale of energy containing eddies in a pipe of diameter D (Hinze, 1959). Based on these arguments and assumptions, the following relation was derived by Hinze (1955)

$$d_{max}\left(\frac{\rho_c}{\sigma}\right)^{3/5} \bar{e}^{2/5} = C = 0.725. \tag{3}$$

The constant 0.725 was obtained by fitting to experimental data of various liquid–liquid dispersions (Clay, 1940) and corresponds to $We_{crit} = \rho_c u'^2 d_{max}/\sigma = 1.17$. This critical Weber number was shown to be in agreement with the value predicted theoretically by considering the resonance frequencies of liquid drops (Sevik and Park, 1973).

In pipe flow, the mean rate of energy dissipation, $\bar{e}$ is related to the frictional pressure drop (expressed in terms of a friction factor f)

$$\bar{e} = \frac{4\tau U_c}{D\rho_c(1-\varepsilon_d)} = \frac{2U_c^3 f}{D}\,\frac{\rho_m}{\rho_c(1-\varepsilon_d)}. \tag{4}$$

Then, Hinze's correlation becomes

$$\left(\frac{d_{max}}{D}\right)_0 = 0.55\left(\frac{\rho_c U_c^2 D}{\sigma}\right)^{-0.6}\left[\frac{\rho_m}{\rho_c(1-\varepsilon_d)}f\right]^{-0.4}. \tag{5}$$

It is to be noted that for high fluid rates, where drops' or bubbles' dispersions develop, the drift velocity between the dispersed and continuous phases is negligible. In this case, the homogeneous

no-slip model is applicable, whereby the in-situ holdup is determined by the superficial velocities of the dispersed and continuous phases ($U_{ds} = Q_d/A$, $U_{cs} = Q_c/A$)

$$\varepsilon_d = \frac{U_{ds}}{U_{ds} + U_{cs}}, \quad \rho_m = \varepsilon_d \rho_d + (1 - \varepsilon_d)\rho_c, \tag{6.1}$$

$$U_c = U_d = U_{ds} + U_{cs} \equiv U_m. \tag{6.2}$$

Correlations for the friction factor in smooth or rough conduits can be used in (5) to calculate d_{max}. For instance, Blasius equation ($f = 0.046/Re_c^{0.2}$) yields

$$\left(\frac{d_{max}}{D}\right)_0 = 1.88\left[\frac{\rho_c(1-\varepsilon_d)}{\rho_m}\right]^{-0.4} We_c^{-0.6}\, Re_c^{0.08}, \quad 1.8Re_c^{-0.7} < \left(\frac{d_{max}}{D}\right)_0 < 0.1, \tag{7}$$

where $Re_c = \rho_c D U_c/\eta_c$ and $We_c = \rho_c U_c^2 D/\sigma$.

Although the turbulence field in pipe flow is not homogeneous and isotropic, Eq. (5) has been proven to yield a good prediction of the maximal drop size in the flow of dilute dispersions for a variety of two-fluid systems, as long as $d_{max} < 0.1D$ (i.e., Kubie and Gardner (1977); Karabelas (1978)). It is to be noted that previous studies considered dilute dispersions, hence $\rho_c(1-\varepsilon_d)/\rho_m \simeq 1$ was assumed. In dispersed bubble flow $\rho_m \simeq \rho_c(1-\varepsilon_d)$ and this assumption holds also for non-dilute dispersions. For liquid–liquid systems, where $\rho_c \simeq \rho_d$, this approximation is valid for $\varepsilon_d \ll 1$. In gas–liquid mist flow, however, the liquid forms the dispersed phase and $\rho_c(1-\varepsilon_d)/\rho_m \simeq (\rho_G/\rho_L)(1-\varepsilon_L)/\varepsilon_L$. The value of this term significantly deviates from the one already for very small holdup of entrained liquid drops.

2.2. Extension of Hinze's model for dense dispersions

The Hinze model (Eqs. (5) and (7)) considers the stability of a single drop in a turbulent field. Therefore, the model may be valid only for dilute dispersions. In dense dispersions, droplet coalescence takes place. Under such conditions, the incoming flow of the continuous phase (at rate Q_c) should carry sufficient turbulent energy to disrupt the tendency to coalesce and to disperse the other phase, which flows at a rate Q_d. The (minimal) rate of surface energy thus formed is given by

$$\dot{E}_s = \frac{\pi d_{max}^2 \sigma}{\pi d_{max}^3/6}\, Q_d = \frac{6\sigma}{d_{max}} Q_d. \tag{8}$$

The rate of surface energy production of the dispersed phase is proportional to the rate of turbulent energy supply by the continuous phase

$$\frac{\rho_c u'^2}{2} Q_c = C_H \frac{6\sigma}{d_{max}} Q_d, \tag{9}$$

where C_H is a constant, $C_H = O(1)$. Substituting (2.1) and (4) yields

$$\left(\frac{d_{max}}{D}\right)_\varepsilon = 2.22 C_H^{3/5}\left(\frac{\rho_c U_c^2 D}{\sigma}\right)^{-0.6}\left[\frac{\rho_m}{\rho_c(1-\varepsilon_d)} f\right]^{-0.4}\left(\frac{\varepsilon_d}{1-\varepsilon_d}\right)^{0.6}. \tag{10}$$

With Blasius equation for f, Eq. (10) reads

$$\left(\frac{d_{\max}}{D}\right)_{\varepsilon} = 7.61 C_{\mathrm{H}}^{3/5} We_{\mathrm{c}}^{-0.6} Re_{\mathrm{c}}^{0.08} \left(\frac{\varepsilon_{\mathrm{d}}}{1-\varepsilon_{\mathrm{d}}}\right)^{0.6} \left[1 + \frac{\rho_{\mathrm{d}}}{\rho_{\mathrm{c}}} \frac{\varepsilon_{\mathrm{d}}}{1-\varepsilon_{\mathrm{d}}}\right]^{-0.4} \tag{11.1}$$

provided

$$1.82 Re_{\mathrm{c}}^{-0.7} < \left(\frac{d_{\max}}{D}\right)_{\varepsilon} < 0.1. \tag{11.2}$$

Thus, given a two-fluid system and operational conditions, the maximal drop size is the largest of the two values obtained via (7,11.1)

$$\frac{d_{\max}}{D} = \mathrm{Max}\left\{\left(\frac{d_{\max}}{D}\right)_0 \left(\frac{d_{\max}}{D}\right)_{\varepsilon}\right\}. \tag{12}$$

It is of interest to note that the empirical correction suggested by Calderbank (1958) for the effect of the dispersed phase holdup on the maximal drop bubble size was to multiply the RHS of (5) and (7) (with $\rho_m/\rho_{\mathrm{c}}(1-\varepsilon_{\mathrm{d}}) \simeq 1$) by $f(\varepsilon_{\mathrm{d}}) = 1 + b\varepsilon_{\mathrm{d}}^a$. The parameter values a = 0.5 and b = 5.72 were suggested by fitting to his experimental data. The similarity with the 0.6 power of ε_{d} in (11.1) and (11.2) implies that such a correlation can reasonably describe the increase of $d_{\max}$ with ε_{d} for some range of $\varepsilon_{\mathrm{d}} > 0$.

2.3. Criterion for transition to dispersed flow

The transition to dispersed flow pattern takes place when the continuous phase turbulence is sufficiently intense to break the dispersed phase into droplets smaller than the critical size, d_{crit}. Thus the transitional criterion is

$$d_{\max} \leqslant d_{\mathrm{crit}} \tag{13}$$

provided $Re_{\mathrm{c}} \geqslant 2100$ and $1.82 Re_{\mathrm{c}}^{-0.7} < d_{\mathrm{crit}}/D < 0.1$.

In dilute dispersions, $Q_{\mathrm{d}} \ll Q_{\mathrm{c}}$, the flow rate of the continuous phase should be raised to a value where the momentum of turbulent eddies is sufficient to meet the criterion (13) with $d_{\max}$ obtained via Hinze's model (7). With increasing Q_{d}, the same turbulence level in the continuous phase can be achieved with lower Q_{c}. However, this turbulence level, which is sufficient to produce a drop with $d_{\max} < d_{\mathrm{crit}}$ in a dilute dispersion, may be incompatible with the high-flow rates of the dispersed phase. A higher rate of turbulent kinetic energy (higher Q_{c}) is required to meet the criterion (13) with $d_{\max}$ evaluated via (11.1) and (11.2).

The critical drop diameter, d_{crit} required for applying (13) can be estimated similarly to the suggestion made by Barnea (1987)

$$\frac{d_{\mathrm{crit}}}{D} = Min\left(\frac{d_{\mathrm{c}\sigma}}{D}, \frac{d_{\mathrm{c}b}}{D}\right) \tag{14}$$

Here $d_{\mathrm{c}\sigma}$ represents the maximal size of drop diameter above which drops are deformed (Brodkey, 1969)

$$\tilde{d}_{c\sigma} = \frac{d_{c\sigma}}{D} = \left[\frac{0.4\sigma}{|\rho_c - \rho_d| g \cos\beta' D^2}\right]^{1/2} = \frac{0.224}{(\cos\beta')^{1/2} Eo_D^{1/2}}, \tag{15.1}$$

$$Eo_D = \frac{\Delta\rho g D^2}{8\sigma}, \quad \beta' = \begin{cases} |\beta|, & |\beta| < 45^\circ, \\ 90 - |\beta|, & |\beta| > 45^\circ \end{cases} \tag{15.2}$$

and d_{cb} is the maximal size of drop diameter above which migration of the drops towards the tube walls due to buoyant forces takes place

$$\tilde{d}_{cb} = \frac{d_{cb}}{D} = \frac{3}{8}\frac{\rho_c}{|\Delta\rho|}\frac{fU_c^2}{Dg\cos\beta} = \frac{3}{8} f \frac{\rho_c}{\Delta\rho g} Fr_c, \quad Fr_c = \frac{U_c^2}{Dg\cos\beta}, \tag{16}$$

where β is the inclination angle to the horizontal (positive for downward inclination). The value of β' in (15.1) and (15.2) reflects the notion that in horizontal and lightly inclined tubes, drops' distortion results mainly from the lateral gravity force (pushing the drops towards the (upper or lower) tube wall), whereas in vertical and off-vertical inclined tubes, drops distortion is due to the axial buoyant force. It is to be noted, however, that the inclusion of $(\cos\beta')^{1/2}$ in $d_{c\sigma}$ is not critical, since its effect is of the order of uncertainty in the value of the constant parameter (0.224) in (15.1).

Criterion (13), with (12) and (14), yields a complete transitional criteria to dispersed flow. When the fluid flow rates are sufficiently high to maintain a turbulence level where $d_{max} < d_{c\sigma}$ and $d_{max} < d_{cb}$, spherical non-deformable drops are formed and creaming of the dispersed droplets at the upper or lower tube wall is avoided. Thus, the dispersed flow pattern is stable.

The values of the numeric constants used for modeling $d_{c\sigma}$ and d_{cb} (0.4 and 3/8 in (14,11.1,11.2), respectively) are not strict and can be turned to better fit experimental data available for a particular system. Higher values of d_{crit} yield lower critical Q_c. Also, the constant C_H may require some tuning. A value of $C_H > 1$ reflects a situation where not all the turbulent kinetic energy in the continuous phase is available for dispersing the other phase (Q_c increases proportionally to $C_H^{0.54}$. In the framework of (13), a tuning of C_H represents the combined effects of the constants used in modeling d_{max} and d_{crit}, therefore $C_H < 1$ should not be ruled out. If not stated otherwise, $C_H = 1$ is assumed.) In the following, the model consisted of criterion (13) with (7,11.1,15.1,16) is denoted by the H-model.

In applying the H-model, the restrictions that define its validity range should not be ignored. The first inherent restriction is that the predicted fluids flow rates along the transitional boundary correspond to turbulent flow of the continuous phase ($Re_c > 2100$). Additional restrictions are due to the turbulence model used by Hinze (1955), which limit the model applicability range to conditions where $1.8\, Re_c^{-0.7} < \tilde{d}_{max} = \tilde{d}_{crit} < 0.1$. With $d_{crit} = d_{c\sigma}$, the lower bound corresponds to $Eo_D < 1.5 \times 10^{-2} Re_c^{1.4}$. It is worth noting at this point that, according to Kolmogorov (1949), for $\eta_d/\eta_c \gg 1$, viscous shear is negligible when $\tilde{d}_{max} \gg l_k(\nu_d/\nu_c)^{3/4}$, in which case the lower bound is replaced by $\tilde{d}_{max} > 1.8 Re_d^{-0.7}$, or $Eo_D < 1.5 \times 10^{-2} Re_d^{1.4}$. Since both Re_d and Re_c are based on mixture velocity, the lower bound is satisfied along the dispersed flow boundary in most practical applications and is to be considered only for extremely viscous oils. The upper bound, however, corresponds to $Eo_D \cos\beta' > 5$, which restricts the applicability of the model to systems of large Eötvös numbers. For terrene gas–liquid systems, this restriction limits the applicability of the H-model to sufficiently large diameter tubes ($D > 1.7$ cm for atmospheric air–water systems). In

liquid–liquid systems, or reduced gravity two-fluid systems, the minimal tube diameter for which the H-model is applicable is even larger.

It is important to note that in case a viscous fluid is considered to form the dispersed phase, the critical Weber number (hence, $d_{\max}$) increases. This is due to the additional amount of energy which is needed to overcome the internal viscous dissipation, induced by drop deformation and mixing within the drop. According to Hinze (1955), effect of the dispersed phase viscosity is represented by the Ohnesorge number, $On = \eta_d/(\rho_d \sigma d_{\max})^{0.5}$. For non-vanishing On, the constant in (3) (and (9)) should be augmented by the term $[1 + f(On)]$. For the critical conditions, $d_{\max} \simeq d_{c\sigma}$, $On \simeq (\eta_d^4 \Delta\rho g/\rho_d^2 \sigma^3)^{0.25} = N_{vd}^{0.25}$. This viscosity number (Morton number of the dispersed phase) includes only the physical properties of the two-fluid system. In systems where the value of N_{vd} is significant, the critical conditions depend also on this dimensionless parameter. However, in the lack of sufficient data for determining the functional dependence N_{vd}, it is suggested that the constants of the H-model should be tuned (augmented) when applied to systems of significant N_{vd}.

In the following section, application of the H-model to systems of large Eo_D is demonstrated. The bounds on the parameter range where this model is valid are further detailed by considering also cases where criterion (13) is applied with $d_{crit} = d_{cb}$ (rather than with $d_{c\sigma}$).

2.4. Application of H-model for systems of $Eo_D > 5$

2.4.1. Dispersed bubble boundary

The application of the transitional criteria for obtaining the dispersed bubble boundary in gas–liquid systems is demonstrated with reference to Tables 1 and 2. In this case the continuous phase is water ($U_{cs} \equiv U_{WS}$) and the dispersed phase is air ($U_{ds} \equiv U_{GS}$).

Table 1 shows the results for a vertical tube of 2.5 cm. For vertical (and off-vertical inclined) systems, $\cos\beta \to 0$ and $d_{c\sigma} < d_{cb}$. Therefore, $d_{crit} = d_{c\sigma}$ is used in criterion (13). As shown in Table 1, for high U_{GS}, the use of Hinze's model (7) for $d_{\max}$ in criterion (13) yields lower values for the minimal U_{WS} required for sustaining a stable dispersion than those obtained using $(d_{\max})_\varepsilon$. Hence, the transitional liquid flow rates are predicted with $\tilde{d}_{\max} = (\tilde{d}_{\max})_0$ up to $U_{GS} \simeq 0.15$ m/s, thereafter model (11.1) ($\tilde{d}_{\max} = (\tilde{d}_{\max})_\varepsilon$) should be used.

Table 2 shows the results obtained for a horizontal tube. For low air flow rates, $\tilde{d}_{cb} < \tilde{d}_{c\sigma}$ and $(\tilde{d}_{\max})_0 > (\tilde{d}_{\max})_\varepsilon$. Hence, criterion (13) with $\tilde{d}_{crit} = \tilde{d}_{cb}$ and $\tilde{d}_{\max} = (\tilde{d}_{\max})_0$ is valid up to $U_{GS} \simeq 0.21$ m/s. For 0.2 m/s $< U_{GS} <$ 0.7 m/s, where $(\tilde{d}_{\max})_\varepsilon > (\tilde{d}_{\max})_0$ and $\tilde{d}_{cb}$ is still smaller than $\tilde{d}_{c\sigma}$, criterion (13) is applied with $\tilde{d}_{\max} = (\tilde{d}_{\max})_\varepsilon$ and $\tilde{d}_{crit} = \tilde{d}_{cb}$. For higher air flow rates, $\tilde{d}_{cb} > \tilde{d}_{c\sigma}$ and the transitional water velocity is obtained with $\tilde{d}_{\max} = (d_{\max})_\varepsilon$ and $\tilde{d}_{crit} = \tilde{d}_{c\sigma}$. It is to be noted that the $\varepsilon_d \to 0$ transitional boundary predicted with $(\tilde{d}_{\max})_0$ (with either $\tilde{d}_{c\sigma}$ or $\tilde{d}_{cb}$) corresponds to a constant mixture velocity ($U_c \equiv U_{ds} + U_{cs} \equiv U_{GS} + U_{WS}$), which is the minimal mixture velocity for transition to dispersed flow.

Comparisons between the predicted curve for transition to dispersed bubble flow and available experimental data for horizontal, inclined and vertical air–water flows are shown in Figs. 1–3. As shown, in all cases the model provides a reasonable prediction of the locus of transition ($C_H = 1$ is used, although a better fit could have been obtained by $C_H \simeq 1.5$–2). Fig. 3 shows that for vertical tube of $D = 5.1$ cm (and larger diameters), the region of dispersed bubble flow at low U_{GS} merges with the region of bubbly flow obtained at low liquid flow rates. Therefore, only

Table 1
Dispersed bubble boundary in upward air–water flow $D = 2.5$ cm, $\tilde{d}_{c\sigma} = d_{c\sigma}/D = 0.067$

U_{GS} (m/s)	Criterion	0.01	0.02	0.05	0.1	0.2	0.5	1	2	5	10	20	50
U_{WS} (m/s)	$(\tilde{d}_{max})_0 = \tilde{d}_{c\sigma}$	**1.72**	**1.71**	**1.68**	**1.63**	1.53	1.23	0.73	–	–	–	–	–
U_{WS} (m/s)	$(\tilde{d}_{max})_\varepsilon = \tilde{d}_{c\sigma} = \tilde{d}_{c\sigma}$	0.64	0.81	1.10	1.37	**1.70**	**2.21**	**2.60**	**2.91**	**2.95**	**2.53**	**1.80**	**0.92**

Table 2
Dispersed bubble boundary in horizontal air–water flow $D = 2.5$ cm

Criterion	U_{GS} (m/s)	0.01	0.02	0.05	0.1	0.2	0.5	1	2	5	10
$(\tilde{d}_{max})_0 = \tilde{d}_{c\sigma}$	U_{ws} (m/s)	1.72	1.71	1.68	1.63	1.53	1.23	0.73	–	–	–
	$\tilde{d}_{c\sigma}$	0.067	0.067	0.067	0.067	0.067	0.067	0.067	–	–	–
$(\tilde{d}_{max})_\varepsilon = \tilde{d}_{c\sigma}$	U_{WS} (m/s)	0.64	1.81	1.10	1.37	1.70	2.21	**2.60**	**2.91**	2.95	2.53
	$\tilde{d}_{c\sigma}$	0.067	0.067	0.067	0.067	0.067	0.067	**0.067**	**0.067**	**0.067**	**0.067**
$(\tilde{d}_{max})_0 = \tilde{d}_{cb}$	U_{ws} (m/s)	**2.42**	**2.41**	**2.38**	**2.33**	**2.23**	1.93	1.43	0.43	–	–
	$\tilde{d}_{cb}$	**0.046**	**0.046**	**0.046**	**0.046**	**0.046**	0.046	0.046	0.046	–	–
$(\tilde{d}_{max})_\varepsilon = \tilde{d}_{cb}$	U_{ws} (m/s)	1.41	1.58	1.82	2.02	2.20	**2.35**	2.30	1.95	0.77	0.10
	$\tilde{d}_{cb}$	.0175	0.022	0.029	0.036	0.045	**0.061**	0.08	0.11	0.218	0.597

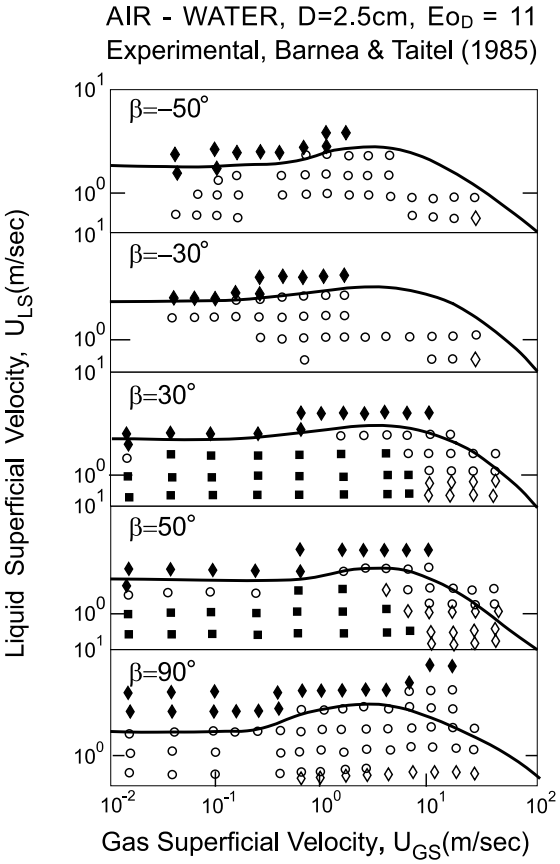

Fig. 2. Comparison of the H-model predictions with experimental data (Barnea and Taitel, 1985) for air–water flow in inclined tubes ($D = 2.5$ cm, $Eo_D = 11$).

$(d_{\max})_{\varepsilon}$(with $d_{\text{crit}} = d_{c\sigma}$) is practically relevant for predicting the transition to dispersed bubble flow via criterion (13). Conditions for the existence of bubbly flow pattern in vertical and off-vertical inclined gas–liquid systems were suggested by Taitel et al. (1980) and Barnea et al. (1985) and have been revised in Brauner (1999).

From a practical point of view, the effect of the tube diameter on the locus of transition is of particular interest for up-scaling laboratory data to larger diameters encountered in field operations.

For low flow rates of the dispersed phase, criterion (13) is applied with $d_{\max} = (d_{\max})_0$. When $d_{\text{crit}} = d_{c\sigma}$ it yields

$$U_c = U_{ds} + U_{cs} = 2.65\left\{\frac{(|\Delta\rho| g\cos\beta')^{0.5}\sigma^{0.1}}{\rho_c^{0.52}\eta_c^{0.08}}D^{0.48}\right\}^{0.893} \equiv 2.65F_{H\sigma}^{0.893}, \tag{17}$$

which predicts that for low $U_{ds}(\to 0)$, superficial velocity of the continuous phase at transition to dispersed flow increases proportionally to $D^{0.43}$ (flow rate is proportional to $D^{2.43}$). When d_{cb} prevails, criterion (13) with (7) and (16) yields

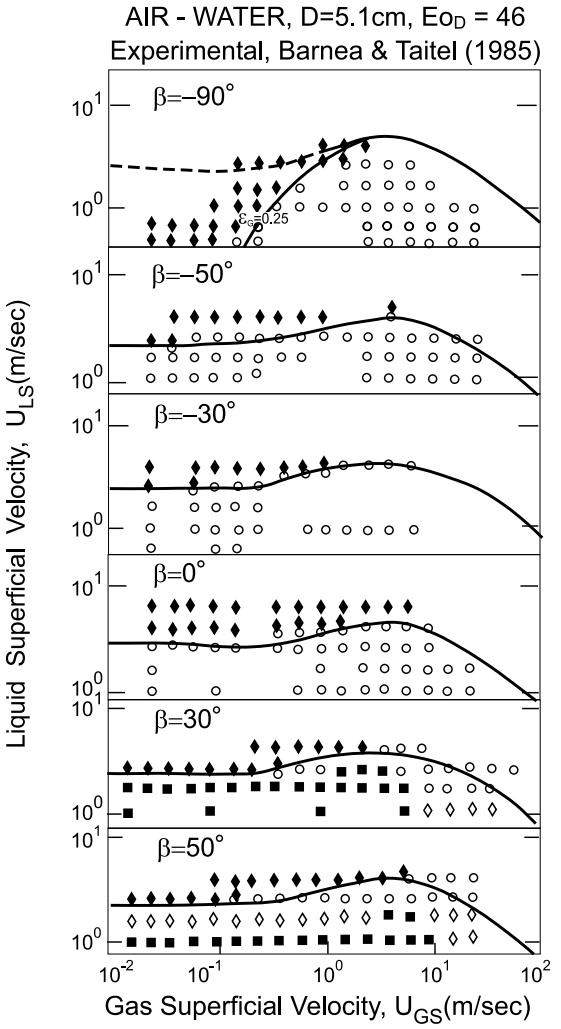

Fig. 3. Comparison of the H-model predictions with experimental data for air–water flow in $D = 5.1$ cm tube ($Eo_D = 46$).

$$U_c = 5\left[\frac{\Delta\rho g \cos\beta\sigma^{0.6}}{\rho_c^{1.32}\mu_c^{0.28}}D^{0.68}\right]^{0.342} = 5F_{Hb}^{0.342} \tag{18}$$

implying a slightly lower effect of tube diameter (U_{cs} increases proportionally to $D^{0.233}$) and slightly higher sensitivity to surface tension and density difference. It is to be noted, however, that d_{cb} increases with U_c, and thus, with increasing $D, d_{cb} > d_{c\sigma}$ already for low U_{ds}. The condition under which $d_{c\sigma}/d_{cb} \leqslant 1$ evolves by substituting (18) in (16)

$$\frac{d_{c\sigma}}{d_{cb}} \simeq 2(N_{vc}\cos\beta)^{-0.00685}\left(\frac{\sigma}{D^2|\Delta\rho|g\cos\beta}\right)^{0.1096}\left(\frac{\cos\beta}{\cos\beta'}\right)^{1/2} \leqslant 1, \tag{19.1}$$

where

$$N_{\mathrm{vc}} = \frac{\eta_{\mathrm{c}}^4 \Delta\rho g}{\rho_{\mathrm{c}}^3 \sigma^3} = \frac{8 We_{\mathrm{c}}^2 Eo_D}{Re_{\mathrm{c}}^4} \tag{19.2}$$

is the viscosity (Morton) number of the continuous phase. For air bubbles dispersed in water, Eq. (19.1) indicates that d_{cb} becomes irrelevant for predicting the transitional boundary in tubes of $D \geqslant 14$ cm. For inclined tubes, it becomes irrelevant already for smaller diameter tubes.

At higher flow rates of the dispersed phase, Tables 1 and 2 and Figs. 1–3 imply that the transition to dispersed bubble flow is associated with a maximum in the continuous phase (water) flow rate. For instance, for air–water flow in a 2.5 cm tube, Table 1 and Fig. 1 show that the maximal water rate for transition to dispersed bubble is obtained at $U_{\mathrm{GS}} \simeq 3.5$ (m/s) with $U_{\mathrm{WS}} \simeq 3.0$ (m/s). For higher water flow rates, the dispersed flow pattern is predicted to be stable irrespective of the air flow rate. The maximal flow rate of the continuous phase along the transitional boundary is obtained at the point where $\mathrm{d}U_{\mathrm{cs}}/\mathrm{d}U_{\mathrm{ds}} = 0$. For dispersed gas bubbles, criterion (13) with $\tilde{d}_{\max} = (d_{\max})_{\varepsilon}$ and $d_{\mathrm{crit}} = d_{c\sigma}$ corresponds to the following relation between the flow rates along the transitional boundary

$$(U_{\mathrm{cs}} + U_{\mathrm{ds}})^{1.12} \left(\frac{U_{\mathrm{cs}}}{U_{\mathrm{ds}}}\right)^{0.6} = 12\, C_{\mathrm{H}}^{3/5} F_{\mathrm{H}\sigma}, \tag{20}$$

where $F_{\mathrm{H}\sigma}$ incorporates all the other system parameters (see (17)). This yields

$$(\varepsilon_{\mathrm{d}})_{\max\{U_{\mathrm{cs}}\}} = 0.536; Max\{U_{\mathrm{cs}}\} = 4.6 C_{\mathrm{H}}^{0.54}; F_{\mathrm{H}\sigma}^{0.893} = U_{\mathrm{cs}}^{*}. \tag{21}$$

Similarly, criterion (12) with $\tilde{d}_{\max} = (d_{\max})_{\varepsilon}$ and $d_{\mathrm{crit}} = d_{cb}$ yields

$$(\varepsilon_{\mathrm{d}})_{\max_{\{U_{\mathrm{cs}}\}}} = 0.205; U_{\mathrm{cs}}^{*} = Max\{U_{\mathrm{cs}}\} = 4.8\, C_{\mathrm{H}}^{0.2}\, F_{\mathrm{H}b}^{0.342}. \tag{22}$$

It is to be noted, however, that since d_{cb} increases with the mixture flow rate, at high U_{ds} (and high U_{cs}) $d_{cb} > d_{c\sigma}$ also for horizontal tubes of small diameter (as demonstrated in Table 2). Therefore, the predicted maximal continuous phase velocity is practically always defined by (21). The diameter effect in (21) is $U_{\mathrm{cs}}^{*} \propto D^{0.43}$, identical to that indicated by (17) for low U_{ds}.

2.4.2. Dispersed flow boundaries in oil–water systems

The application of transitional criterion (13) for predicting the transition to $D_{\mathrm{O/W}}$ or $D_{\mathrm{W/O}}$ in oil–water systems is demonstrated in Figs. 4–7 in comparison with the experimental data of Trallero (1995), Guzhov et al. (1973) and Simmons et al. (1998) obtained in horizontal tubes and with the experimental data of Flores et al. (1997) obtained in vertical tubes. In these figures, boundary 4 corresponds to the results of the H-model when applied with water as the continuous phase (oil is dispersed, $U_{\mathrm{cs}} \equiv U_{\mathrm{WS}}, U_{\mathrm{ds}} \equiv U_{\mathrm{OS}}$), whereas boundary 5 is obtained when the H-model is applied with oil as the continuous phase (water is dispersed, $U_{\mathrm{cs}} \equiv U_{\mathrm{OS}}$ and $U_{\mathrm{ds}} \equiv U_{\mathrm{WS}}$). In these figures, a rough tuning of $C_{\mathrm{H}}(C_{\mathrm{H}} = 0.5\text{–}2)$ is suggested to better represent the trends in the data. However, since the critical velocity is proportional to $C_{\mathrm{H}}^{0.5}$, such a variation in C_{H} has a minor effect on the locus of the transitional boundaries, which may be practically insignificant in view of the ambiguity involved in defining the exact location of the transition to fully dispersed flow in oil–water systems. It is worth noting that for the critical flow rates along boundary 4, the mixture

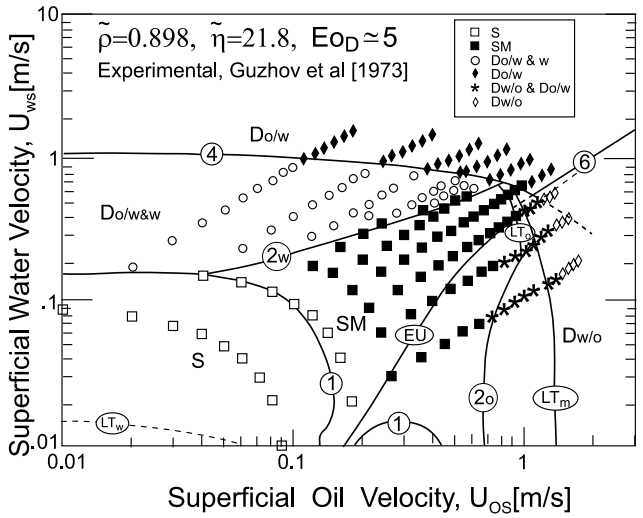

Fig. 4. The H-model predictions for transition to $D_{O/W}$ (boundary 4, $C_H = 0.5$) and transition to $D_{W/O}$ (boundary 5) in horizontal oil–water system of $Eo_D \simeq 5$. Comparison with experimental data of Guzhov et al. (1973). Other boundaries (Brauner, 1998): 1 – neutral stability boundary for smooth stratified flow; 2w, 2o – Upper limit on stratified flow configuration; 6 – dispersion inversion line (Eq. (24)); EU – equal velocity of fluids in stratified layers; LT_o – laminar/turbulent transition in the oil layer.

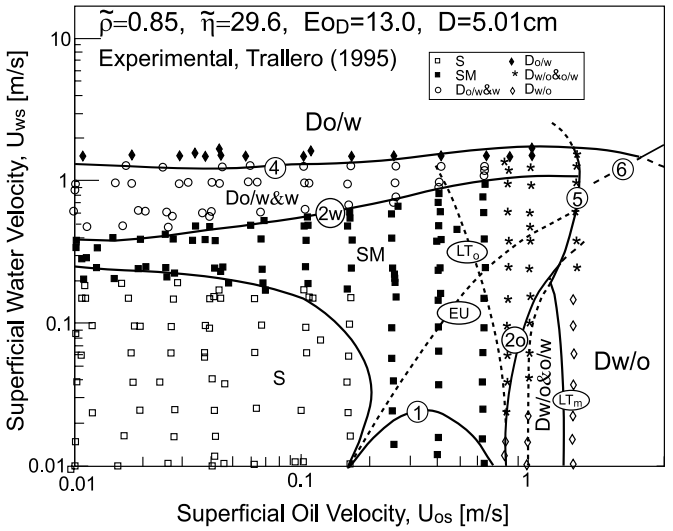

Fig. 5. The H-model predictions ($C_H = 2$) for transition to $D_{O/W}$ (boundary 4) and transition to $D_{W/O}$ (boundary 5) in horizontal oil–water system of $Eo_D \simeq 13$. Comparison with experimental data of Trallero (1995).

Reynolds number is already sufficiently high to assure turbulent flow in water. However, when a viscous oil forms the continuous phase, locus of the transition to $D_{W/O}$ may be constrained by the minimal flow rates required for transition to turbulent flow in oil ($Re_c = 2100$ along boundary LT_m). As shown in Figs. 4,5,7, this is the situation for relatively low water rates, where the liquid

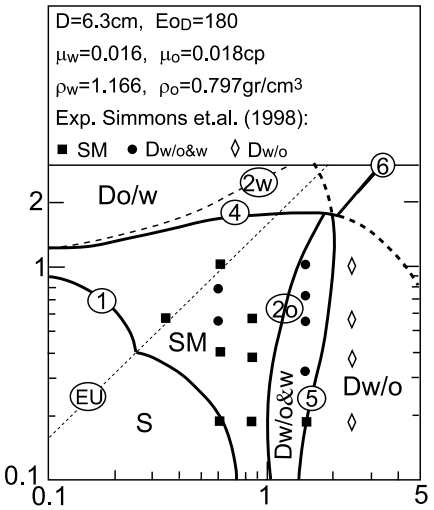

Fig. 6. The H-model predictions for transition to $D_{O/W}$ (boundary 4) and transition to $D_{W/O}$ (boundary 5) in horizontal oil–water system of $Eo_D \simeq 180$. Comparison with experimental data of Simmons et al. (1998).

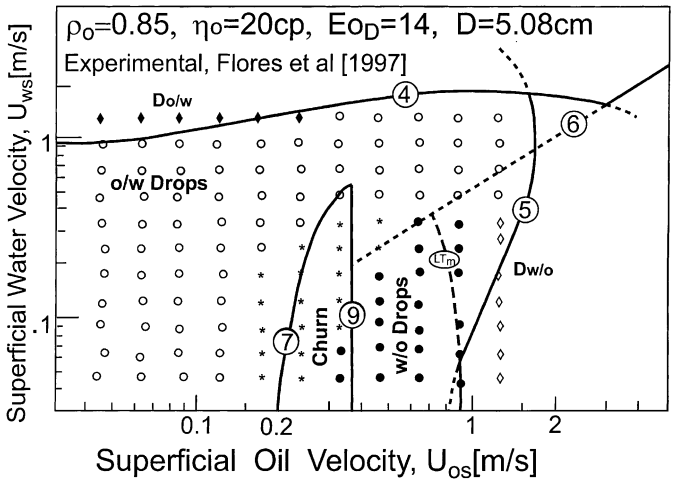

Fig. 7. The H-model predictions ($C_H = 2$) for transition to $D_{O/W}$ (boundary 4) and transition to $D_{W/O}$ (boundary 5) in vertical upward oil–water flow, $Eo_D = 14$: Comparison with experimental data of Flores et al. (1997). The modeling of churn flow (boundaries 7 and 9) is given in Brauner (1998).

flow rates predicted by the H-model along boundary 5 correspond to laminar flow of the mixture. The required turbulent dispersive forces exist only beyond the LT_m boundary, which therefore forms a part of the $D_{W/O}$ transitional boundary. The prediction of other flow pattern boundaries shown in these figures and the notation are detailed in Brauner (1998) (see also the detailed notation in Fig. 4).

For air–water systems, when water form the continuous phase, (21) predicts the maximal water superficial velocity where a flow pattern other than the dispersed bubbles may be stable. In liquid–liquid systems, where $\rho_d \simeq \rho_c$, the maximal U_{cs} is shifted to lower ε_d. It can be shown that when $\rho_d = \rho_c$, Eq. (21) is replaced by

$$(\varepsilon_d)_{U_{cs}^*} = 0.395, \quad U_{cs}^* = 3.71 C_H^{0.54} F_{H\sigma}^{0.893}. \tag{23}$$

In oil–water systems, when water forms the continuous phase $U_{cs} \equiv U_{WS}, U_{ds} \equiv U_{OS}$ Eq. (23) yields the critical water superficial velocity U_{WS}^* above which criterion (13) predicts a stable o/w dispersion, irrespective of the oil rate; whereas with $U_{cs} \equiv U_{OS}$ and $U_{ds} \equiv U_{WS}$ (23) predicts the critical oil superficial velocity, U_{OS}^* beyond which, in view of (13), a dispersion of w/o is stable for all U_{WS}. Thus, for $U_{OS} > U_{OS}^*$ and $U_{WS} > U_{WS}^*$, the flow pattern is a dispersed flow. In this region, the flow patterns of dispersion of w/o ($D_{W/O}$) and dispersion of oil in water ($D_{O/W}$) share a common boundary. The transition between these two patterns takes place along the phase inversion curve. Along this curve, the continuous and dispersed phases spontaneously invert (Yeh et al. (1964), Arirachakaran et al. (1989), Nädler (1995), Mewes et al. (1998), Angeli and Hewitt (1996)). It is the locus of the phase inversion curve which completes the definition of the regions of stable $D_{W/O}$ and $D_{O/W}$. Hence, the maximal holdup of either a stable $D_{W/O}$ or $D_{O/W}$ is controlled by the phase inversion phenomena.

The transition from $D_{O/W}$ to $D_{W/O}$ in these maps (boundary 6) is calculated by applying Arirachakaran et al. (1989) correlation for the critical water cut, $\dot{\varepsilon}_W^I$ at phase inversion

$$\dot{\varepsilon}_W^I = \left(\frac{U_{WS}}{U_{WS} + U_{OS}}\right)_I = 0.5 - 0.1088 \ \log_{10}(\eta_o/\eta_r); \quad \text{or } U_{OS} = U_{WS}\frac{1 - \varepsilon_W^I}{\varepsilon_W^I} \tag{24}$$

with $\eta_r = 1$ mPa s. For oils viscosities above ≈ 0.2 Pa s, a constant value of $\dot{\varepsilon}_W^I \simeq 0.15$ was reported based on the experiments carried out with agitated oil–water dispersions (Brocks and Richmond, 1994). This correlation reflects experimental evidences that by increasing the oil viscosity, its tendency to be dispersed increases and lower holdup of water phase, ε_W is required to invert $D_{W/O}$ to $D_{O/W}$ (the critical oil holdup for inversion increases). Hence, the maximal dispersed phase holdup cannot be bounded by an a priori determined constant (based on the consideration of maximal package density of constant diameter spheres, say $\varepsilon_d = 0.52$) which would be applicable to any two-fluid system. The maximal holdup is not determined by geometrical constraints, since the drops are not of uniform size, but rather by the physical properties of the two fluids involved. The phase inversion phenomena and its modeling are the subject of a subsequent paper.

2.4.3. Annular-mist boundary

In gas–liquid systems, the annular-mist pattern can be considered as the analog of w/o dispersion in liquid–liquid systems. The gas flow rates required for stabilizing the annular-mist pattern can, in principle, be predicted by applying the transitional criteria to dispersed flow with gas (air) as the continuous phase and liquid (water) as the dispersed phase. The model predictions are demonstrated in Fig. 8 for horizontal and vertical tubes. In this figure, boundary 5 describes the critical flow rates predicted by the H-model for stabilizing a dispersion of water drops in a continuous air phase (boundary 4 is a segment of the transitional boundary to dispersed bubbles

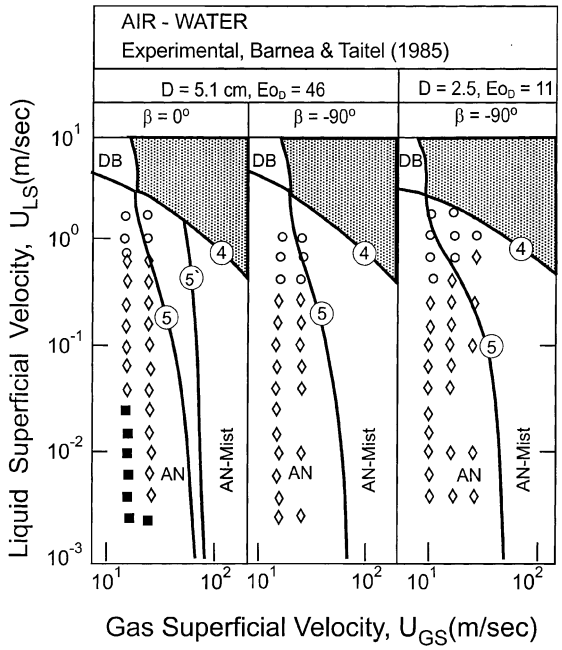

Fig. 8. The critical flow rates required for transition to mist flow. 5 – H-model applied with $d_{crit} = d_{c\sigma}$; 5′ – H-model applied with $d_{crit} = d_{cb}$.

shown in Figs. 1–3). Indeed, very high air superficial velocities are needed for dispersing water into fine droplets, which seem to be beyond the range of the experimental data in these figures. This boundary must not be interpreted as the locus for the onset of drops' atomization, which occurs at lower gas–flow rates ($U_{GS} \simeq 20$ m/s in atmospheric air–water system, independently of the tube diameter, Brauner, 2000), but rather as the conditions for stabilizing a fully developed mist flow due to turbulent dispersive forces. It is to be noted, however, that in contrast to w/o dispersions (where the momentum of water drops is insufficient for penetrating through the continuous oil phase and for wetting the tube walls) in gas–liquid systems, impingement of water drops on the walls keeps the tube walls wetted. Therefore, no clear distinction can be made between the annular and the annular-mist patterns, the transition is rather gradual, and the annular–mist is usually considered a sub-regime of annular flow. The presence of a water film effects an increase in the friction factor, in which case, the Blasius friction factor correlation can significantly underestimate the turbulent energy dissipated in the gas core. With augmentation of the friction factor, the boundary of the mist flow (shown in Fig. 8) will shift towards lower gas rates.

It is further worth noting that a decline in the gas critical flow rate by increasing the liquid flow rate as indicated by boundary 5 in Fig. 8, evolves from criterion (13) applied with (7). It essentially results from an increase of the mixture density with increasing amounts of entrained liquid droplets. In horizontal tubes (Fig. 8(a)), the H-model predicts that the transitional boundary to mist flow is controlled by $d_{crit} = d_{cb} (< d_{c\sigma}$, boundary 5′). The application of criterion (13) with $d_{crit} = d_{c\sigma}$ yields lower critical gas flow rates (boundary 5). The Experimental data are needed in order to judge which of the models for d_{crit} is more relevant. The phase inversion (DB-to-annular-

mist transition) is expected in the ambivalent region, where the H-model predicts that both a dispersion of bubbles-in-water and dispersion of water-in-air are stable (indicated in Fig. 8 by the shaded area). It takes place at very high gas and liquid rates, beyond the range where the visual characterization of flow patterns was attempted. This transition may not be indicated by an abrupt change in the continuous phase, but rather by the coexistence of regions of $D_{G/W}$ and $D_{W/G}$ in the flow field.

2.4.4. The H-model validity range

As discussed in Section 2.3, validity of the H-model is limited to systems of $Eo_D \cos\beta' > 5$. This limitation evolves due to restriction on the turbulence model used in Hinze's model, (drops/bubbles smaller than the inertial sub-range scale, 0.1D) applied on a critical drop size represented by $d_{c\sigma}$. For horizontal (or slightly inclined) systems and low mixture flow rates, where the critical drop size is characterized by d_{cb}, the restriction $\tilde{d}_{cb} < 0.1$ corresponds to $Eo_D > 2.31 N_{vc}^{0.0176} (\cos\beta)^{-0.982}$ (see (19.1) and (19.2)). For horizontal air–water systems, this extends somewhat to the range of tube diameters for which the H-model is applicable at low mixture velocities (from $D > 1.7$ cm corresponding to $Eo_D > 5$ to $D > 0.95$) cm. However, since at higher mixture velocities, $d_{c\sigma}$ is the critical size, the criterion $Eo_D > 5$ is used to define the range where the H-model is applicable for predicting the transition to dispersed flow.

It is of interest to note at this point that the value of $Eo_D = 5$ represents a threshold value also for transition to surface tension dominant region in the rise velocity of Taylor bubbles (Brauner, 1999). In unhindered gravitational motion of drops and bubbles through liquids, the Eötvös number is based on the drop diameter, however, $Eo_d = \triangle\rho g d^2/8\sigma = 5$ represents a threshold value for transition from ellipsoidal regime to spherical-cap drops/bubbles regime (Clift et al., 1978).

3. Criterion based on Hughmark (1971) model (K-model)

3.1. Model equations

For drop sizes greater than the energy containing eddies ($\tilde{d}_{max} > 0.1$), Hughmark (1971) has suggested that the dynamic pressure due to the turbulent field should be evaluated based on fluctuating turbulent velocity. In pipe flow, the fluctuating turbulent velocity is of the order of the friction velocity, $u*$

$$\left(u'^2\right)^{1/2} \propto u* = \left(\frac{\tau}{\rho_c}\right)^{1/2} = U_c \left(\frac{f}{2}\right)^{1/2}, \tag{25}$$

where τ is the wall shear stress. Replacing (2.1) and (2.2) by (25) and assuming that the critical Weber number is the same as that predicted by Hinze's (1955) model ($We_{crit} = 1.17$), Kubie and Gardner (1977) have obtained the following model for d_{max} in a dilute dispersion

$$(\tilde{d}_{max})_o = 1.38\, We_c^{-1} f^{-1}, \quad 0.1 < \tilde{d}_{max} < 1. \tag{26}$$

In non-dilute dispersions, the wall shear stress is modeled by $\tau = 1/2 f \rho_m U_c^2$, accordingly the RHS of (26) should be multiplied by ρ_c/ρ_m. Following the arguments of Section 2.3, for dense dispersions, this turbulence model can be used in the energy balance (9), which considers the production rate of the dispersed phase surface energy in comparison to the supply rate of turbulent energy by the continuous phase. Taking $u_\theta'^2 \simeq u_r'^2 \simeq u_x'^2 \simeq U_c\,(0.5 f \rho_m/\rho_c)^{1/2}$, the rate of turbulent energy supply is modeled by

$$\dot{E}_k \simeq \frac{3}{4}\rho_m U_c^2 f Q_c. \tag{27}$$

In this case, the condition, $\dot{E}_k \simeq \dot{E}_s$ yields

$$\left(\frac{d_{max}}{D}\right)_\varepsilon = 8 C_K\, We_c^{-1}\, f^{-1}\, \frac{\rho_c}{\rho_m}\left(\frac{\varepsilon_d}{1-\varepsilon_d}\right), \tag{28}$$

where C_K is a constant, $C_K = O\{1\}$. When the Blasius correlation for the friction factor in used in (26) and (28), these read

$$(\tilde{d}_{max})_0 = 30\frac{\rho_c}{\rho_m} We_c^{-1} Re_c^{0.2}, \tag{29.1}$$

$$(\tilde{d}_{max})_\varepsilon = 174 C_K\, We_c^{-1} Re_c^{0.2}\frac{\rho_c}{\rho_m}\left(\frac{\varepsilon_d}{1-\varepsilon_d}\right). \tag{29.2}$$

Thus, in applying criterion (12) for two-fluid systems of $Eo_D < 5$, the models (29.1) and (29.2) replace (7) and (11.1), respectively. As with the H-model, here too, a transitional criterion is obtained by comparing the resultant d_{max} with the critical drop sizes defined by (14,15.1,16). It is to be noted, however, that d_{cb} is irrelevant for systems of $Eo_D < 5$, since when U_c along a transitional boundary (predicted with d_{cb} as a critical size) is substituted back to the model for d_{cb} (16), the resultant expression reads

$$\tilde{d}_{cb} = \tilde{d}_{max} = C/Eo_D^{1/2}. \tag{30}$$

The constant C is similar (however larger) than that used in (15.1) and (15.2). Therefore, here, the only relevant critical drop scale is that defined by $d_{c\sigma}$, and the transitional criterion to dispersed flow is

$$\tilde{d}_{max} \leqslant \tilde{d}_{c\sigma} \tag{31.1}$$

with

$$\tilde{d}_{max} = Max\left\{\left(\tilde{d}_{max}\right)_0, \left(\tilde{d}_{max}\right)_\varepsilon\right\} \tag{31.2}$$

where $(\tilde{d}_{max})_0$, $(\tilde{d}_{max})_\varepsilon$ are given by (29.1) and (29.2). This model is denoted as the K-model. It is applicable to systems of $Eo_D < 5$, corresponding to $\tilde{d}_{c\sigma} > 0.1$. It is to be noted, however, that when $d_{c\sigma} \geqslant D$, the only relevant scale for characterizing the critical drop size is that of the tube diameter. Considering $\tilde{d}_{c\sigma}$ as a relevant scale as long as $\tilde{d}_{c\sigma} < 0.5$ limits the relevance of the K-model to systems of $0.2 < Eo_D < 5$.

3.2. The K1-model

For systems of $Eo_D < 0.2$, the critical drop size is scaled with D. Taking $d_{crit} \simeq 0.5D$, yields the following transitional criterion:

$$Max\left\{\left(\tilde{d}_{max}\right)_0\left(\tilde{d}_{max}\right)_\varepsilon\right\} \leqslant \frac{1}{2}, \quad Eo_D < 0.2, \quad Re_c > 2100. \tag{32}$$

In view of (29.1,29.2,32) in systems of small Eötvös numbers, the transition to dispersed bubbles is determined in terms of: $We_c, Re_c, \tilde{\rho}$ and ε. Model (32) is denoted as the $K1$-model.

3.3. Application of the K-model and K1-model to systems of $Eo_D < 5$

The significance of using the K-model (rather than the H-model) for systems of $Eo_D < 5$ is demonstrated with reference to Figs. 9 and 10. These figures show the effect of tube diameter on

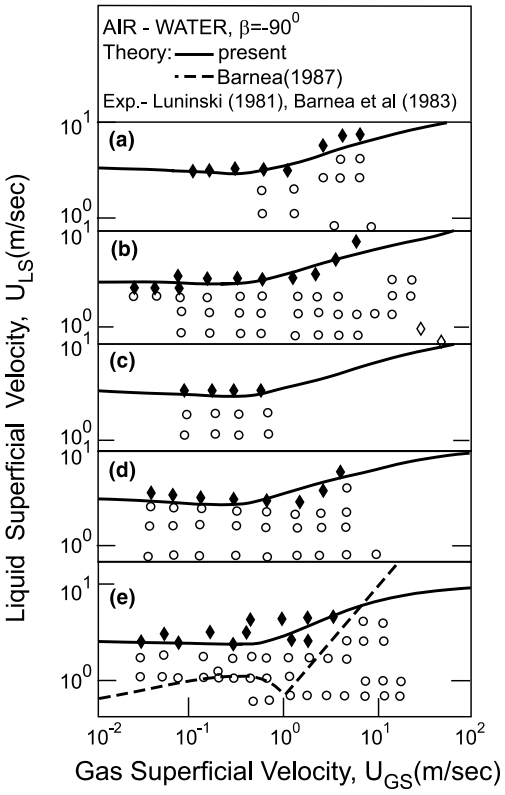

Fig. 9. Comparison of the K-model predictions with experimental data for upward air–water flow in vertical tubes, $0.2 < Eo_D < 5$: (a) $D = 1.23$ cm, $Eo_D = 2.6$; (b) $D = 0.985$ cm, $Eo_D = 1.7$; (c) $D = 0.815$ cm, $Eo_D = 1.2$; (d) $D = 0.615$ cm, $Eo_D = 0.66$; (e) $D = 0.4$ cm, $Eo_D = 0.28$.

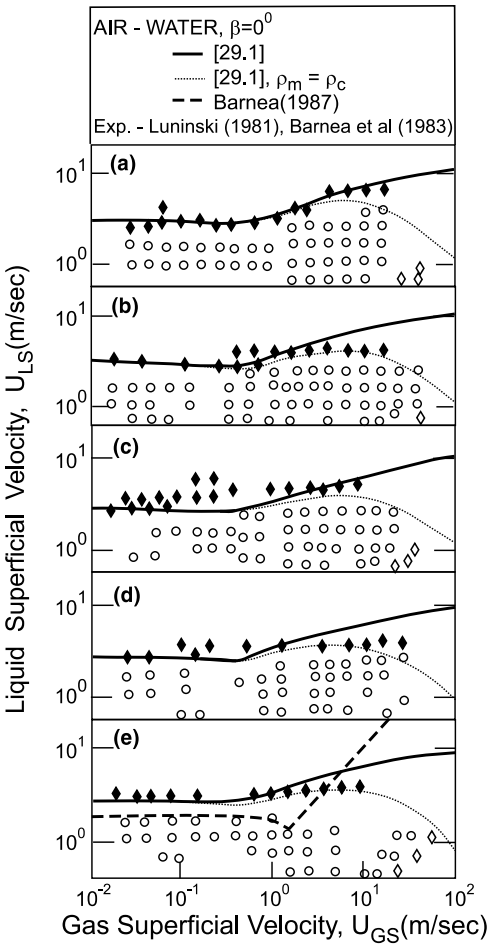

Fig. 10. Comparison of the K-model predictions with experimental data for air–water flow in horizontal tubes, $0.2 < Eo_D < 5$: (a) $D = 1.23$ cm, $Eo_D = 2.6$; (b) $D = 0.985$ cm, $Eo_D = 1.7$; (c) $D = 0.815$ cm, $Eo_D = 1.2$; (d) $D = 0.615$ cm, $Eo_D = 0.66$; (e) $D = 0.4$ cm, $Eo_D = 0.28$.

the locus of transition to dispersed bubble for air–water flow in small diameter, vertical and horizontal tubes. In air–water flow, $Eo_D < 5$ corresponds to $D < 1.7$ cm. The effect of tube diameter indicated by the K-model is evident by expressing the transitional boundary in terms of dimensional variables. In the range of low flow rates of the dispersed phase ($\varepsilon_d \to 0$), criterion (31.1) is applied with $(d_{max})_0$, (29.1). In this case, flow rates along the transitional boundary are given by

$$U_c = U_{ds} + U_{cs} = 8.53\left[\frac{\left(\sigma\Delta\rho g\cos\beta'\right)^{0.5} D^{0.2}}{\rho^{0.8}\eta^{0.2}}\right]^{1/1.8} = 8.53F_{k\sigma}^{0.555} \tag{33}$$

provided $Re_c > 2100$. Eq. (33) predicts that for low U_{ds} ($\equiv U_{GS}$), the superficial velocity of the continuous phase, $U_{cs} \equiv U_{WS}$ at transition increases proportionally to $D^{0.11}$ (compared to $D^{0.43}$ predicted by the H-model). Thus, the K-model predicts an almost negligible effect of the tube diameter. This is confirmed in view of the comparison with the experimental data (Luninski, 1981; Barnea et al., 1983) shown in Figs. 9 and 10. Indeed, down-scaling flow pattern maps from $D \simeq 1$ cm to $D = 0.4$ cm seems to be associated with a negligible variation of the locus of the transition to dispersed bubble flow. Barnea (1987) model tends to underpredict the critical water velocity for transition to dispersed flow in small diameter tubes (as demonstrated in Fig. 9(e). This model is inapplicable to the range of small D, since it yields $\tilde{d}_{max} = O(1)$ or even larger than one). Application of the H-model for down-scaling would also significantly underpredict the critical water flow rates. It is of interest to note that the K-model shows a significantly higher sensitivity to surface tension, as expected for systems of low Eo_D.

At higher flow rates of the dispersed phase (higher U_{GS} in Figs. 9 and 10) the transitional criterion (31.1) is applied with $(d_{max})_{\varepsilon}$, (29.2). For low pressure air–water systems, $\rho_c/\rho_m \simeq (1-\varepsilon_d)^{-1}$, in which case the model predicts a monotonous increase in the critical water flow rate with increasing the air flow rate. For horizontal systems (Fig. 10), the model tends to over prediction of the observed critical water flow rates. The results obtained when the wall shear stress is modeled assuming $\rho_m \equiv \rho_c$ are also shown in Fig. 10 (dotted line). The experimental boundary seems to fall in between these two approximations (implying that the effect of the holdup in dense air dispersion can be represented in (29.2) by $\varepsilon_d/(1-\varepsilon_d)^m$, $0 < m < 1$). It is to be noted that the results shown in Figs. 9 and 10 were obtained with $C_K = 1$. Obviously a better fit with experiments can be obtained by tuning the value of C_K when applied to a specific system (U_{cs} increases proportional to $C_K^{0.56}$).

The restriction that $d_{c\sigma}$ represents the critical drop (or bubble size) as long as $\tilde{d}_{c\sigma} < 0.5$ limits the applicability of the K-model in air–water systems to tube diameters larger than $D \simeq 0.35$ cm. For capillaries of $D < 0.35$ cm ($Eo_D < 0.2$), the K1-model ($d_{crit} \simeq 0.5D$) is suggested and is given by criterion (32). For low U_{ds}, where $(d_{max})_0$ prevails, (32) reads:

$$U_c = U_{ds} + U_{cs} = \left(\frac{\sigma}{\rho_c^{0.8}\,\eta_c^{0.2}\,D^{0.8}}\right)^{1/1.8} = 9.72\,F_{K1}^{0.555} \tag{34}$$

which indicates that for low U_{ds}, the critical U_{cs} increases with reducing the tube diameter proportionally to $D^{-0.44}$ (provided Re_c corresponds to turbulent flow). Thus, in capillaries, the effect of tube diameter is predicted to be opposite to that obtained at large diameter (large Eo_D systems). The prediction of the K1-model is in agreement with the experimental results of air–water-flow in 1.097 mm tube (Triplett et al., 1999) which is shown in Fig. 11. It is to be noted that boundary 3 in the figure is the criterion suggested for the existence of bubbly flow in capillaries ($Eo_D < 0.2$ and $\varepsilon_d < 0.2$–0.25) and $(U_m)_{crit}$ is the critical mixture velocity for obtaining areated liquid slugs (Brauner, 1999).

For even smaller tube diameters, the mixture velocity predicted by (34) may not be sufficient to obtain turbulent flow. In this case, the K1-model is no longer relevant. The flow rate of the continuous phase should be increased to a level which results in turbulent flow, where the required dispersive forces exist. At low U_{ds}, the K1-model becomes irrelevant when

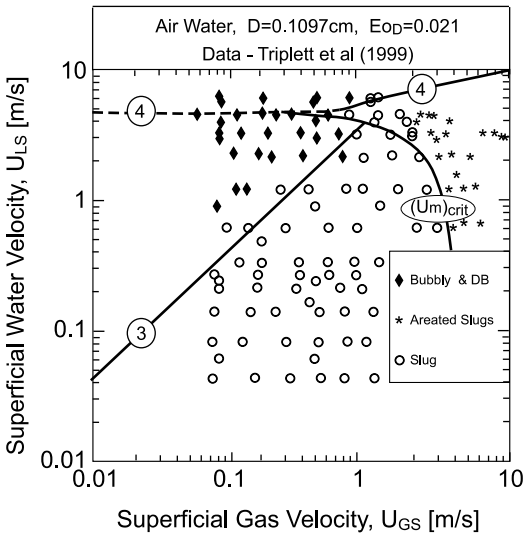

Fig. 11. Comparison of the K1-model predictions with experimental data for air–water flow in capillary tube, $Eo_D = 0.021$.

$$Re_c = \frac{9.72\rho_c D F_{K1}^{0.55}}{\eta_c} \leqslant (Re_c)_{L/T}, \tag{35.1}$$

For $(Re_c)_{L/T} = 2100$ it corresponds to

$$\frac{\rho_c \sigma D}{\eta_c^2} < 16,000, \quad Eo_D < 0.2. \tag{35.2}$$

For air–water system (35.2) corresponds to $D < 0.22$ mm ($Eo_D < 8 \times 10^{-3}$). For such small (micro) tubes, the closure laws for the friction factor may be different from the conventional relations used for macrotubes (see, for example, Mala and Li, 1999). However, with viscous liquids (as a continuous phase) criterion (35.2) is met for larger D. For $D < 16000\eta_c^2/(\rho_c\sigma)$, the transition to fully dispersed (emulsified) flow is constrained by the locus laminar/turbulent transition ($U_{cs} \propto D^{-1}$, as discussed also with reference to the transition to $D_{W/O}$ in Figs. 4–7).

It is to be noted, however, that in systems of $\tilde{d}_{c\sigma} \geqslant 1 (Eo_D < 0.05)$, the region of low U_{ds} corresponds to bubbly (drops) flow also in the range of low U_{cs} (see Fig. 11). Therefore, the transition from bubbly flow to dispersed flow may not be distinct. At higher U_{cs}, where transition from intermittent/slug flow to dispersed bubble flow takes place, the K1-model is applied with $(d_{max})_\varepsilon$, resulting in higher continuous phase flow rate (and mixture flow rate) than those obtained by (34). Thus, in this region the K1-model is applicable to smaller D than that indicated by (35.2)).

4. Effect of tube diameter on transition to dispersed bubble flow

The varying trend of the effect of tube diameter on the critical velocity of the continuous phase is further demonstrated in Fig. 12. The figure summarizes the minimal critical mixture velocity for

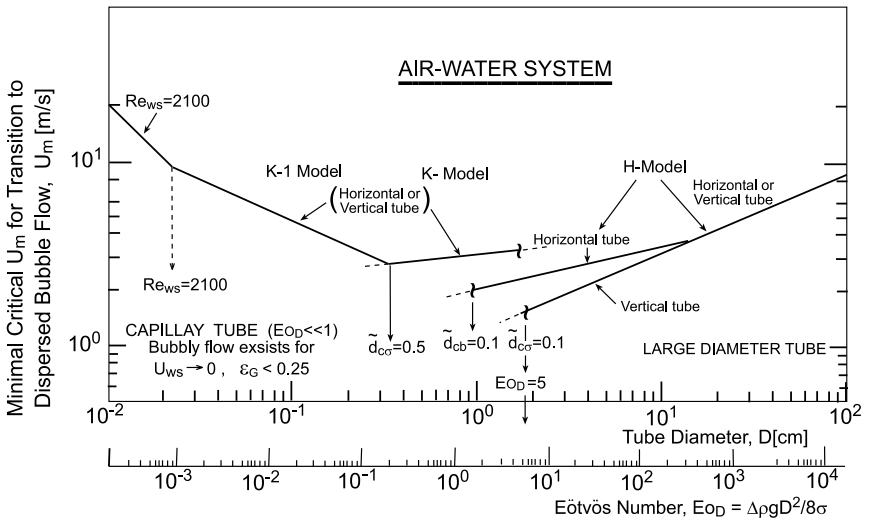

Fig. 12. The effect of the Eötvös number on the minimal mixture velocity required for establishment of dispersed bubble flow in terrestrial air–water systems.

transition to dispersed air bubbles in atmospheric air–water systems as predicted by the various models in the range of their applicability. This critical velocity corresponds to the water superficial velocity in the limit $U_{GS} \to 0$ ($\varepsilon_G \to 0$). For the sake of convenient interpretation, dimensional scales are used in the figure.

Air–water systems of $Eo_D > 100$ can be considered as large diameter tubes, where the tube inclination has no effect on transition also for low air flow rates and the critical water velocity increases with increasing D proportionally to $D^{0.43}$. On the other hand, capillary tubes are associated with $Eo_D < 0.1$, where the critical velocity decreases with increasing D. The lowest critical water rates are predicted in the range $Eo_D \simeq 1$–10, where some ambiguity exists regarding the discontinuous transfer between the H-model and the K-model. The discontinuity is more pronounced for vertical tubes. Apparently, this problem could have been resolved by extending the range of the K-model to higher Eötvös numbers. But, the K-model significantly overpredicts the critical water rates in vertical tubes of $Eo_D > 5$. Inspection of Figs. 1 and 9(a) indicates roughly a doubling of the critical water superficial velocity in 1.23 cm vertical tube ($Eo_D \simeq 2.7$) compared to that observed in 2.5 cm tube ($Eo_D = 11$). This implies a possible physical justification for the gap between the above two models, which evolves from the change in the characteristic turbulent scales. However, more data are required for deciding whether (and how) the numeric constants used in the models (those in the turbulent models for d_{max} and in the models of d_{crit}) should be tuned to provide a smooth transition between the K-model and the H-model.

5. Summary and conclusions

The prediction of drop size limitation in dense dispersions is essential for modeling dispersed flow boundaries. To this aim, the Kolmogorov (1949)–Hinze (1955) model for break-up droplets

in turbulent flow is revised. It is suggested that energy considerations can be employed for estimating the maximal drop size in dense dispersions. The limitation imposed by the turbulence model used by Hinze (1955) is also considered and for size drop/bubble larger than 0.1D, the Hughmark (1971)–Kubie and Gardner (1977) model is employed.

Based on the revised and extended models, a unified approach for predicting the transition to dispersed flow patterns in gas–liquid and liquid–liquid systems is suggested. In gas–liquid systems, these include the dispersed-bubble and annular-mist flows; whereas, in liquid–liquid systems, the boundaries of o/w and w/o dispersions (emulsions) are considered. Comparisons with the experimental data available from the literature indicate that the models are capable of predicting the dispersed flow boundaries in a variety of two-fluid systems over a wide range of fluids' physical properties, tube diameter and inclination.

These models indicate that the locus of transition to fully dispersed flow is determined by several dimensionless parameters, which include the flow Reynolds number, the Weber number, the Eötvös number, the fluid flow rates ratio, density ratio (for $\rho_d/\rho_c \gg 1$) and viscosity ratio (for $\eta_d/\eta_c \gg 1$). However, the range where each of the models is applicable is defined in terms of the Eötvös number, $Eo_D = \Delta\rho g D^2/8\sigma$. Upon examining the effect of the tube diameter on the critical flow rates required for establishing dispersed flow in air–water systems, a non-monotonic trend is suggested. In large diameter tubes ($Eo_D > 100$), the critical mixture velocity phase increases with increasing the tube diameter whereas in capillaries ($Eo_D < 0.1$), an opposite trend is predicted. This implies that the up-scaling of data should be approached with care.

References

Angeli, P., Hewitt, G.F., 1996. Pressure gradient phenomena during horizontal oil–water flow. ASME Proc. OMAE 5, 287–295.

Arirachakaran, S., Oglesby, K.D., Malinowsky, M.S., Shoham, O., Brill, J.P., 1989. An analysis of oil/water flow phenomena in horizontal pipes. In: SPE Paper 18836, SPE Prof. Prod. Operating Symp., Oklahoma.

Barnea, D., 1987. A unified model for predicting flow-pattern transitions for the whole range of pipe inclinations. Int. J. Multiphase Flow 11, 1–12.

Barnea, D., Luninski, Y., Taitel, Y., 1983. Flow pattern in horizontal and vertical two-phase flow in small diameter pipes. Can. J. Chem. Eng. 61, 617–620.

Barnea, D., Shoham, O., Taitel, Y., 1985. Gas–liquid flow in inclined tubes: flow pattern transitions for upward flow. Chem. Engng. Sci. 40, 131–136.

Barnea, D., Taitel, Y., 1985. Flow pattern in two-phase gas–liquid flows. In: Cheremisinoff, J.P. (Ed.), Encyclopedia of Fluid Dynamics. Gulf Publishing.

Brauner, N., 1998. Liquid–liquid two-phase flows. In: Schlunder, E.V., Hewitt G.F. (Eds.), HEDH/HEDU Heat Exchanger Design Update (Section 2.3.5).

Brauner, N., 2000. The onset of drops atomization and the prediction of annular flow boundaries in two-phase pipe flow. Internal Report-S101, Faculty of Engineering, Tel Aviv University, Israel.

Brauner, N., 1999. The prediction of insitu holdup in liquid slugs. Internal Report-S99, Faculty of Engineering, Tel Aviv University, Israel.

Brauner, N., Moalem Maron, D., 1992a. Flow pattern transitions in two-phase liquid–liquid horizontal tubes. Int. J. Multiphase Flow 18, 123–140.

Brauner, N., Moalem-Maron, D., 1992b. Identification of the range of small diameter conduits regarding two-phase flow patterns transitions. Int. Comm. Heat Mass Transfer 1, 29–39.

Brauner, N., Moalem Maron, D., 1998. The effect of surface forces on flow patterns and flow characteristics in two-phase systems. In: Proceedings of the ICHMT International Symposium on Liquid–Liquid Two Phase Flow, Antalya, Turkey, Begell House Inc.

Brauner, N., Moalem Maron, D., Rovinsky, J., 1998. A two-fluid model for stratified flows with curved interfaces. Int. J. Multiphase Flow 24, 975–1004.

Brocks, B.W., Richmond, H.N., 1994. Phase inversion in non-ionic surfactant-oil–water systems – III. The effect of the oil-phase viscosity on catastrophic inversion and the relationship between the drop sizes present before and after catastrophic inversion. Chem. Eng. Sci. 49, 1843–1853.

Brodkey, R.S., 1969. The Phenomena of Fluid Motions. Addison-Wesley, Reading, MA.

Calderbank, P.H., 1958. Physical rate processes in industrial fermentations; Part 1: The interfacial area in gas–liquid contacting with mechanical agitation. Tran. Inst. Chem. Eng. 36, 443–463.

Chen, X.T., Cai, X.A., Brill, J.P., 1997. A general model for transition to dispersed bubble flow. Chem. Eng. Sci. 52, 4373–4380.

Clay, P.H., 1940. The mechanism of emulsion formation in turbulent flow. Proceedings. Akademie van Wetenschappen (Amsterdam) 43, 852–965.

Clift, R., Grace, J.R., Weber, M.E., 1978. Bubbles Drops and Particles. Academic Press, New York, Orlando, London.

Flores, J.G., Chen, X.T., Sarica, C., Brill, J.P., 1997. Characterization of oil–water flow patterns in vertical and deviated wells. In: 1997 SPE Annual Technical Conf. and Exhibition, San Antonio, Texas, SPE Paper 38810, pp. 1–10.

Grace, J.R., Wairegi, T., Brophy, J., 1978. Break-up of drops and bubbles in stagnant media. Can. J. Chen. Engng. 56, 3–8.

Guzhov, A., Grishin, A.D., Medredev, V.F., Medredeva, O.P., 1973. Emulsion formation during the flow of two immiscible liquids. Neft. Choz. (in Russian) 8, 58–61.

Hinze, J., 1955. Fundamentals of the hydrodynamic mechanism of splitting in dispersion processes. AIChE J. 1 (3), 289–295.

Hinze, J., 1959. Turbulence. McGraw-Hill, New York.

Hughmark, G.A., 1971. Drop breakup in turbulent pipe flow. AIChE J. 4, 1000.

Karabelas, A., 1978. Droplet size spectra generated in turbulent pipe flow of dilute liquid/liquid dispersions. AIChE J. 24 (2), 170–180.

Kolmogorov, A.N., 1949. On the breaking of drops in turbulent flow. Doklady Akad. Nauk. 66, 825–828.

Kubie, J., Gardner, G.C., 1977. Drop sizes and drop dispersion in straight horizontal tubes and in helical coils. Chem. Eng. Sci. 32, 195–202.

Luninski, Y., 1981. Two phase flow in small diameters line-flow patterns and pressure drop, Ph.D. Thesis. Tel Aviv University.

Mala, G.M., Li, D.Q., 1999. Flow characteristics of water in microtubes. Int. J. Heat Fluid Flow 20, 142–148.

Mewes, D., Nadler, M., Tukaz, A., 1998. The effect of emulsification on the flow behaviour of two immiscible liquids in horizontal pipes. In: International Symposium on Liquid–Liquid Two-Phase Flow and Transport Phenomena, Antalya, Turkey, Begell House Inc, New York.

Nädler, M., 1995. The pressure losses in multiphase flow of oil, water and gas in horizontal pipes. Ph.D. Thesis, University of Hanover, Fortschritt-Berichte VDI, Reihe 7: Strömungstechnick No. 296.

Sevik, M., Park, S.H., 1973. The splitting of drops and bubbles in turbulent fluid flow. J. Fluid Eng. Trans. ASME 95, 54–59.

Simmons, M.J.H., Azzopardi, B.H., Zaidi, S.H., 1998. Measurements of drop sizes and flow patterns in liquid–liquid pipe flow. In: Proceedings of the ICMF 98, Lyone, France.

Taitel, Y., Barnea, D., Dukler, A.E., 1980. Modeling flow pattern transitions for steady upward gas–liquid flow in vertical tubes. AIChE J. 26, 345–354.

Taitel, Y., Dukler, A.E., 1976. A model for prediction flow regime transition in horizontal and near horizontal gas–liquid flow. AIChE J. 22, 47–55.

Trallero, J.L., 1995. Oil–water flow patterns in horizontal pipes. Ph.D. Thesis, The University of Tulsa, Tulsa.

Triplett, K.A., Ghiaasiaan, S.M., Abdel-Khalik, S.I., Sadowski, D.L., 1999. Gas–liquid two-phase flow in microchannels. Part I: Two-phase flow patterns.. Int. J Multiphase Flow 25, 377–394.

Yeh, G., Haynie Jr., F.H., Moses, R.E., 1964. Phase-volume relationship at the point of phase inversion in liquid dispersions. AIChE. J. 10 (2), 260–265.

Zukoski, E.E., 1966. Influence of viscosity, surface tension and inclination angle on motion of long bubbles in closed tubes. J. Fluid Mech. 25, 821–837.